Growth and Optical Characterization of In-Plane-Ordered AlN Nanowires for UV–C Emitting Devices

Corentin Guérin, Fabien Jourdan, Gwénolé Jacopin, Bruno Daudin

Growth and Optical Characterization of In-plane Ordered AlN Nanowires for UV-C Emitting Devices

Corentin Guérin[1,2,*], Fabien Jourdan[1], Gwénolé Jacopin[2] and Bruno Daudin[1]

[1]Univ. Grenoble Alpes, CEA, Grenoble INP, IRIG, PHELIQS, NPSC, 17 av. des Martyrs, 38000 Grenoble, France

[2] Univ. Grenoble Alpes, Grenoble INP, Institut Néel, SC2G, CNRS, 38000 Grenoble, France.

[*]Corresponding author: corentin.guerin@cea.fr

Abstract

In recent years, solid-state C-ultraviolet emitters (<230nm) have become an important issue for disinfection applications. AlN nanowire-based LEDs could prove to be a very serious option for this purpose. Here, the growth of AlN nanowires by plasma-assisted molecular beam epitaxy on in-plane ordered GaN pedestals is investigated. The influence of growth temperature and Al/active N ratio on the morphology of AlN nanowires puts in evidence the role of Al adatom diffusion length on both the top and the sidewalls. In addition, we found that the relative geometrical arrangement of Al effusion cell and N plasma cell with respect to sample normal drastically affects nanowire morphology, opening the path to the controlled formation of GaN/AlN core/shell nanowire heterostructures. Cathodoluminescence experiments reveal the correlation between near band edge optical signature and nanowire morphology, the sharpest band edge emission peaks corresponding to nanowires grown in migration enhanced epitaxy conditions.

Keywords : AlN, MBE growth, Ordered nanowires, UV-C, Cathodoluminescence

Introduction

Nanowires (NWs) of III-nitride semiconductors exhibit remarkable properties, related to their small diameter, high aspect ratio and large amount of free surface. These specificities lead to enhanced strain relaxation and to the formation of nano-objects free of extended defects, by contrast to the situation observed in layers, for which the lack of adapted substrates and the tendency to columnar growth leads to the formation of a high density of threading dislocations (TDs). Hence, one can view an ensemble of III-nitride NWs as an ensemble of perfect, independent nano-crystals, which can be grown on a large variety of substrates. These remarkable properties make NWs especially attractive for opto-electronic devices realization. The enhanced electrical dopant incorporation in NWs with respect to their layer counterpart [1] and the eased strain relaxation of axial heterostructures [2] are additional assets. More specifically, AlN and (Ga)AlN NWs are well adapted to the elaboration of devices emitting in the UV-C range, i.e. between 200 and 280 nm. Nevertheless, the direct growth of AlN NWs on usual planar substrates was scarcely reported. It requires high temperature conditions [3,4], making preferable the use of bottom-up GaN pedestals as a pseudo substrate for growing ensembles of AlN NWs. Following this strategy, proof of concepts of NW-based UV-C emitting devices was recently reported [5,6]. However, diameter dispersion and random spacing associated to self-nucleated GaN NW template constitute a serious drawback. Such a size dispersion results in inhomogeneous current flow in an ensemble of randomly nucleated NWs, with a fraction of them only contributing to electroluminescence [7]. One way to overcome these limitations is to use patterned substrates to ensure the growth of regularly spaced NWs homogeneous in size. It is the goal of this article to investigate the growth mechanism and the structural and optical properties of such AlN NWs grown on in-plane ordered GaN pedestals elaborated by metalorganic chemical vapour deposition (MOCVD). We show that the morphology of AlN drastically depends on kinetics, which can be tuned by temperature and metal/active nitrogen (Al/N) ratio value. In addition, NW morphology depends on the relative geometrical arrangement of metal and N-plasma cells in the growth chamber. We demonstrate that highest Al adatom mobility associated with migration-enhanced epitaxy (MEE) leads to faceted AlN NWs adapted to the controlled growth of UV-C emitting NW heterostructures.

Methods

The AlN NWs were grown by plasma-assisted molecular beam epitaxy (PA-MBE). The pseudo-substrate consisted of Ga-polar GaN pedestals selectively grown by MOCVD on Si (111). Various GaN pedestal diameters (nominally 115, 130 and 150 nm) were available, with a pitch of 400 and 800 nm. Two growth temperatures (T_G) were investigated, namely 750°C and 950 °C, and the Al/N ratio value varied between 0.2 and 1. The growth time was 1.5 hours for samples with Al/N=0.2 (v_c=0.12ML/s, expressed in equivalent AlN growth rate) and Al/N=1 (v_c=0.60ML/s). Additional samples were grown by Migration Enhanced Epitaxy (MEE), which consists of alternating exposure to Al (20 s) and N (30 s). These parameters were chosen to account for the difference between Al and N fluxes (respectively 0.77 ML/s and 0.60 ML/s) and prevent Al accumulation. One sample consisting of 280 cycles (equivalent growth time of 90 minutes corresponding to total Al exposure) was grown. In addition, a sample consisting of 180 cycles was also grown. The characteristics of the different samples investigated are reported in table 1.

Table 1: list of samples. For MEE samples, the effective growth time corresponds to total N exposure time.

Sample	A	B	C	D	E	E’
Growth Temperature (°C)	950	950	750	750	950	950
Growth time (minutes)	90	90	90	90	90	60
Al/N ratio value	0.2	~ 1	0.2	~ 1	MEE	MEE

It is worth recalling that the Al flux available on the top (0001) surface *a priori* consists of the nominal Al flux directly impinging on top (Φ_{top}) and an additional Al flux resulting from Al impinging on the sidewalls (Φ_{sw}) and diffusing towards the top surface [8]. However, it has to be stressed that the effective *amount* of Al contributing to growth is affected by the sticking coefficient, which depends on both growth temperature and the surface nature, i.e. top surface or sidewalls. Furthermore, as a major difference between layers and NWs, the limited Al adatom mobility implies that the morphology of AlN NW sections is indeed affected by both the rotation speed during growth and the relative geometrical arrangement of N and Al cell in the growth chamber [9]. This issue, particularly critical for adatom kinetics on the sidewalls, was addressed by comparing the morphology of AlN NWs grown using two different Al cells. Al_1 (respectively Al_2) cell was tilted by 20° (respectively 10°) with respect to the substrate normal

direction. In these conditions, the angle between N plasma cell and Al_1 (respectively Al_2) cell is 8° (respectively 18°).

As schematically shown in figure 1f, the c-plane and m-plane growth rate, v_c and v_m, as well as the overall morphology of AlN NWs are directly related to Φ_{top} and Φ_{sw} and to the diffusion length of Al adatoms on the sidewalls and top, which is affected itself by T_G and the Al/ N ratio value. In addition, the Al adatom transfer from sidewalls to top (and vice versa) is governed by the presence of two Ehrlich-Schwöbel barriers (ESB) [10]: ESB_1 preventing Al adatoms diffusing on the c-plane top to diffuse downwards on the sidewall and ESB_2 preventing Al adatoms diffusing upwards on the sidewall to reach the c-plane.

Results and discussion

The results for samples A and B grown at T_G = 950 °C using Al_1 cell are shown in figure 1, putting in evidence the strong variability of AlN NW morphology depending on the Al/N ratio value. Rough NW top surrounded by nano-walls in the periphery is observed (figure 1a) for an Al/N flux ratio value of 0.2 (sample A), while AlN NWs with facetted pyramidal top section are formed (figure 1b) for Al/N ~ 1 (sample B).

Next, samples C and D were grown at T_G = 750°C. For an Al/N flux ratio value of 0.2 (sample C, figure 1c) a rough top is observed. Also, parasitic growth on the sidewalls is indicative of short Al diffusion length. By contrast, for Al/N ~ 1 (sample D, figure 1d), a flat top and smooth sidewalls are observed, suggesting that Al diffusion is mostly governed by Al/N ratio value rather than by growth temperature.

In the case of sample E grown by MEE, the formation of an AlN section with a flat top is observed in figure 1e. Such a flat NW top and the smooth appearance of the sidewalls are consistent with an important increase in the diffusion of Al adatoms. This increase in diffusion is attributed to the metal-rich nature of the MEE growth. Actually, each Al deposition cycle results in the deposition of around 14 metal monolayers on the surface of the sample. When consumed by active N, the surface of the sample remains "metal-rich" until the last layer of aluminium is consumed. The aperture of an efficient diffusion channel on the (0001) surface of GaN in presence of a metallic layer was theoretically put in evidence [11,12]. The formation of an Al contracted bilayer on growing AlN in Al-rich conditions [13] is consistent with the observation of smooth surfaces in MEE conditions, suggesting that a similar mechanism is at play in this case.

Concerning the Al adatom diffusion along the sidewalls, the observation of a crown-shaped shell exhibiting a six-fold symmetry on sample D (see figure 1d) is assigned to the preferential upwards diffusion along the narrow a-plane ridges corresponding to the m-planes intersections. This feature is consistent with theoretical predictions on the anisotropic diffusion mechanisms in the case of GaN NWs [14], again assessing a similar behaviour in the case of AlN, i.e. an easy Al adatom diffusion parallel to [0001] on a-plane ridges. Interestingly, this crown-shaped shell is not seen in the MEE sample in figure 1e, which is assigned to the saturation of the sidewalls with Al during the MEE cycle and the concomitant formation of a homogeneous AlN layer during the N exposure step.

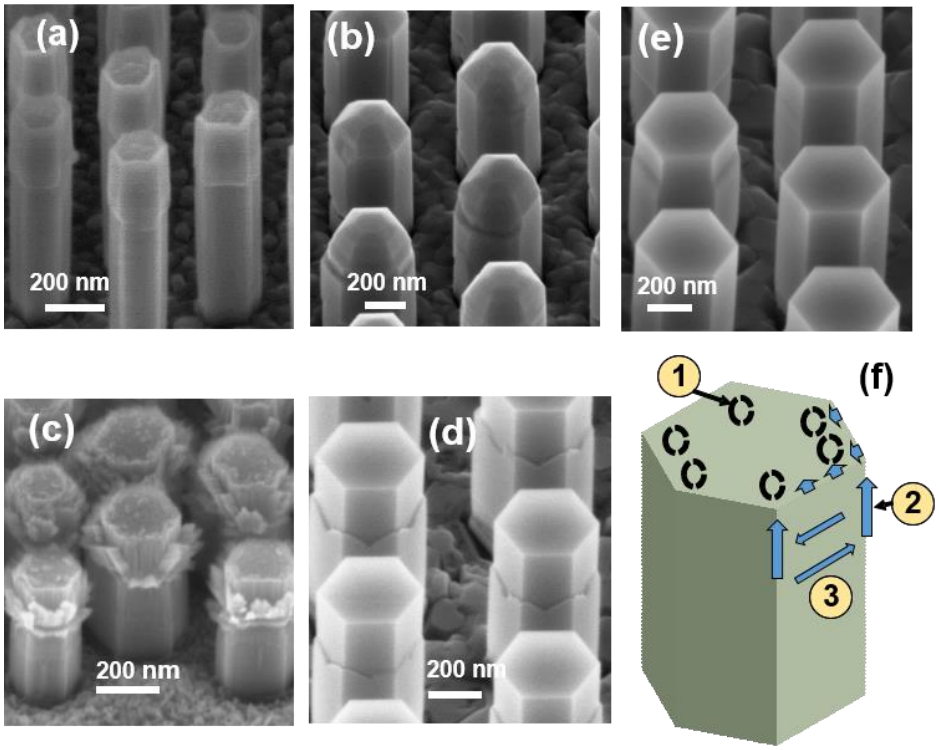

Figure 1: Morphology of AlN NWs depending on growth temperature and Al/N ratio value. (a) sample A: T_G = 950°C, Al/N = 0.2, ; (b)sample B: T_G = 950°C, Al/N = 1, ; (c) sample C: T_G = 750°C, Al/N = 0.2,; (d) sample D: T_G = 750°C, Al/N = 1,; (e) sample E: MEE conditions, at T_G = 950°C,; (f) Schematics of the processes involved in the growth of AlN NWs. Two ESB have to be considered: ESB_1 preventing Al adatoms diffusing on the c-plane top to diffuse downwards on the sidewall and ESB_2 preventing Al adatoms diffusing upwards on the sidewall to reach the c-plane. Accordingly, a maximum Al presence probability is expected in (1), which acts as a nucleation center. Along the sidewalls, easy upwards diffusion is expected along the a-plane ridge (2) while Al diffusion in the m-plane is perpendicular to c-direction (3).

The relevancy of the processes identified in figure 1f is further demonstrated in figure 2 for sample E', which corresponds to a total MEE growth time of 60 minutes at T_G= 950°C. In particular, the increased Al adatom presence probability in the hexagon top corners, which is assigned to ESB_1, may result in a lack of matter in the centre of the growing AlN NW, as sketched in figure 2. Following the peripheral nucleation of flat islands in the corners schematized in figure 2a, the progressive extension of these islands towards the centre eventually leads to the formation of a hole as shown in figure 2b. Consistently with this model, the resulting hole exhibits one hexagonal shape and appears to be rotated by 30 ° with respect to the NW core, as seen in figure 2c. For longer growth time, the central hole eventually disappears, leading to the formation of a flat top, as seen in figure 1e.

Such a phenomenology, namely the peripheral nucleation of successive top layers on the growing NW, is very similar to previous observations on the growth mode of GaN NWs as a function of growth temperature and Ga/N ratio value [15]. Indeed, for both GaN and AlN, theoretical studies have demonstrated the dependence of Ga (resp. Al) adatom diffusion as a function of Ga (resp. Al) coverage, putting in evidence a drastic lowering of diffusion barrier on (0001) surface in metal-rich conditions [11, 12]. The present results confirm that both GaN and AlN exhibit similar trends, with an Al adatom diffusion length on the c-plane depending on both temperature and Al coverage.

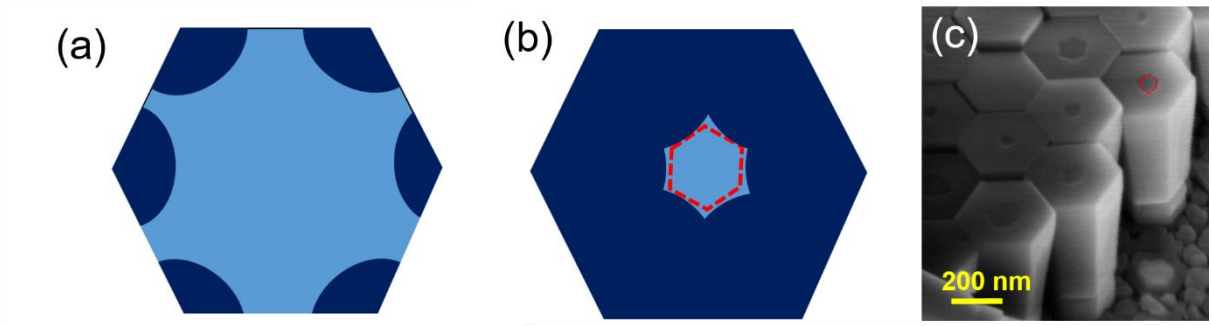

Figure 2: Schematics of AlN growth on c-plane. (a) nucleation occurs at the periphery, due to the increased Al presence probability in the corners of the hexagonal top surface. The nuclei adopt the shape of slabs with m-plane side facets. (b) progressive enlargement of the slabs and their coalescence eventually result in the formation of an hexagonally-shaped hole in the center, which is rotated by 30° with respect to the base, in accordance with (c) experimental results corresponding to sample E' grown by MEE at 950°C during 60 minutes.

Because of the limited Al transfer from m-plane to c-plane put in evidence above, we can infer that the morphology of AlN NWs will depend on the amount of Al directly impinging on top and sidewalls, respectively. In order to address this issue, an additional set of samples was grown using Al_2 cell, which is tilted by 10° with respect to sample normal (see figure 3a). By taking advantage of the chemical contrast between GaN and AlN, SEM observations performed at 20kV on dispersed NWs allowed one to determine both m-plane and c-plane growth rate as illustrated in figure 3b.

We found (see figure 3c) that the ratio between longitudinal and lateral growth rate is drastically affected by the Al cell tilt angle with respect to the normal to the NW top surface. Interestingly, the v_c/v_m growth rate ratio favourably compares with the theoretical calculations reported in table 2, assuming no Al transfer from sidewalls to top and vice versa. This result confirms the role played by ESB_1 and ESB_2 on the kinetics of Al adatoms, assessing a reduced Al transfer, if any, from sidewalls to top, in agreement with the NW morphology results shown in figure 1. It also confirms the poor Al diffusion on m-plane and a-plane ridge in the temperature and Al/N range considered in the present work, excepting the samples grown using MEE.

Noticeably, the ratio v_c/v_m of sample E is slightly lower than for standard conditions growth. However, it is worth stressing that the determination of v_c and v_m in MEE conditions may be biased by the unknown desorption rate of species alternately deposited. In practice, v_c and v_m for sample E were determined by dividing the thickness of longitudinally and laterally grown section, respectively, by the time of exposure to nitrogen. The v_c/v_m value was then calculated assuming the same species desorption rate for top surface and sidewalls.

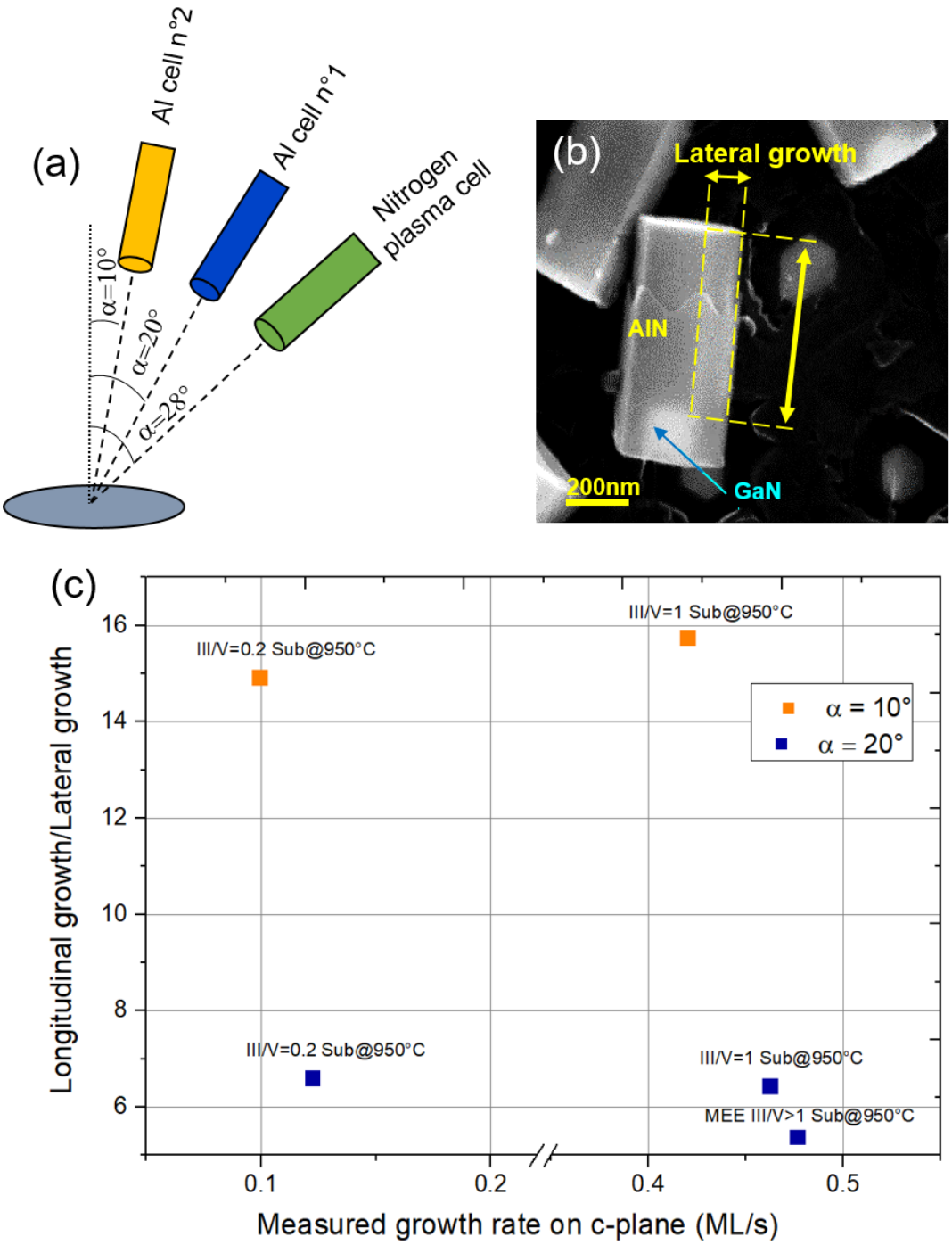

Figure 3: (a) Schematics of cell geometrical arrangement (b) Scanning electron microscopy image of a single AlN/GaN NW, illustrating AlN shell formation around the GaN base, allowing one to experimentally determine v_c/v_m. (c) vc/vm ratio as a function of vc for various Al/N nominal ratios and Al cell orientations.

Table 2 : Calculated dependence on Al cell geometrical arrangement of the ratio of effective Al flux impinging on top (Φ_c) and sidewalls (Φ_m) (see supplementary material for the calculation), measured ratio of Longitudinal/ Lateral growth rate (v_c/v_m) and Al/N ratio on the sidewalls, for an Al/N nominal ratio equal to 1.

Al cell tilt with respect to sample normal	10° (Al2)	20° (Al1)
$\frac{\phi_c}{\phi_m}(calculated)$	17.9	8.6
$\frac{v_c}{v_m}(measured)$	14-16	6-7
$\frac{III}{V}_m(calculated)$	0.33	0.68

As MBE growth is performed at a temperature far lower than the AlN thermodynamic equilibrium one [4] the growth process is expected to be mostly governed by kinetics, emphasizing the role of diffusion on the top surface and on the sidewalls and its influence on the final NW morphology. However, in practice, the independent effect of growth temperature and Al/N ratio value on the diffusion process as well as the different Al/N ratio values for top surface and sidewalls related to cell geometrical arrangement in the growth chamber may lead to a large variety of combinations associated with an extended morphology variability. If focusing on the case of a growth temperature equal to 950°C, the effect of the nominal Al/N flux on morphology is shown in figure 1. For an Al/N ratio of 0.2, we observed the formation of AlN nanotubes (see figure 1a). As schematized in figure 4 (a) and (b), the observation of a rough top surface and the formation of such nanotubes are consistent with both a short diffusion length on c-oriented top and a longer one on the m-oriented sidewalls leading to Al accumulation in their upper part, which eventually leads to nanotube formation. This statement is consistent with the observation in figure 1d and 3b of a crown-shaped shell exhibiting a six-fold symmetry putting in evidence an eased Al upwards diffusion along the a-oriented facets formed at the intersection of m-plane sidewalls, followed by a uniform repartition of Al excess all over the perimeter through an easy diffusion on m-plane perpendicular to c-axis.

In the case of a nominal Al/N ratio on top ~ 1, the large Al adatom diffusion length on the top facet combined to the presence of ESB_1 leads to an increased nucleation probability in

top corner and terrace formation. As schematized in figure 4 (c) and (d), the repetition of this process finally leads to formation of a pyramidal tip, as experimentally shown in figure 1b. Interestingly, in MEE conditions and short growth time, this mechanism is also responsible for the formation of hexagonal holes in the top center facet, as shown in figure 2. For long growth times, the large diffusion length associated with the presence of an Al film on the growing surface eventually leads to a smooth top surface. It is noteworthy that the smoothness of the sidewalls simultaneously observed allows one to predict a diffusion enhancement on m-plane sidewalls also, when covered by an Al film, as shown in figure 1e.

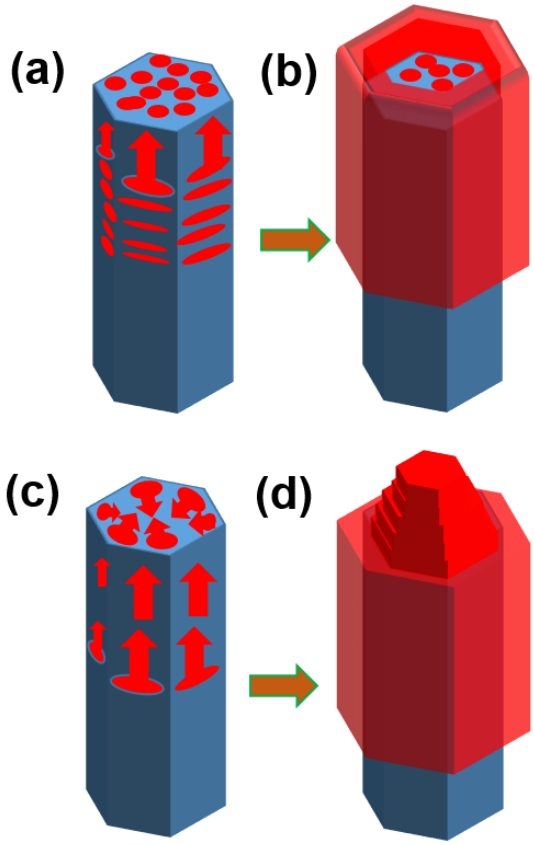

Figure 4: Schematics of AlN NWs growth. (a) For an Al/N ratio = 0.2, short diffusion length on top and sidewalls, leads to (b) rough top surface and sidewalls. Formation of nanotubes is observed, due to peripheral Al accumulation in the upper part of the sidewalls. (c) for an Al/N ratio ~ 1, longer diffusion length on top and along the (11-20) ridge at the intersection of (1-100) m-plane sidewalls leads to (d) a nucleation of successive top layers close to the hexagon corner, leading to pyramid formation. Simultaneously, the increased amount of Al reaching the sidewalls and the enhanced diffusion length in a direction perpendicular to c-axis results in a thick shell with smooth walls.

In order to correlate the morphology with the crystallographic and optical quality, cathodoluminescence (CL) spectroscopy was carried out in a scanning electron microscope (SEM). The acceleration voltage was kept to 5kV to mainly probe the AlN part of the NW. CL spectra have been recorded on a CCD camera coupled to the microscope thanks to a parabolic mirror and with a 550-mm focal length spectrometer equipped with 1800 grooves/mm diffraction grating. Measurements were performed at 5K.

Figure 5a focuses on the near-band-edge emission of AlN. The sample A exhibits a broad band around 5.95eV, as well as a sharp peak at 6.034eV associated with the $\Gamma_5^{(n=1)}$ transition of the free exciton[16]. We tentatively attribute the 5.95eV broadband to donor-acceptor recombination, which is assigned to the poor crystallographic quality of AlN grown in N-rich conditions and/or the presence of a high concentration of impurities. Additionally, a small contribution at 5.650 eV, remains unidentified.

As concerns samples B and D grown at 950 °C and 750°C, respectively, for an Al/N ratio equal to ~ 1, the CL spectra display similar band edge signature as a further evidence that the overall crystallographic and optical properties of AlN NWs are more sensitive to Al/N ratio than to growth temperature in this range. Two sharp peaks are observed at 6.034 eV and 6.007 eV, respectively associated with the $\Gamma_5^{(n=1)}$ recombination of the free exciton and the recombination of the exciton bound to a neutral donor level D^0X_1. Peaks in this energy range were previously reported and assigned to silicon or oxygen shallow donor [16]. The differences in the absolute position of the peaks in figure 5 with respect to reported values in literature are attributed to different internal stress states, originating from the hetero-epitaxial growth on the GaN pillar. A broad contribution around 5.95eV, is present in both spectra of samples B and D grown at stoichiometry.

The spectrum of sample E exhibits drastic differences with respect to other samples. For the $\Gamma_5^{(n=1)}$ peak, a shift of around 10 meV to higher energy, is observed, the same as for D^0X_1, which suggests that the nanowire probed here is more constrained, possibly related to MEE growth mode. Indeed, MEE-grown samples exhibit a larger diameter, associated with formation of a thicker AlN shell, inferred from the lower v_c/v_m value shown in figure 3c. This is expected to affect the strain balance between AlN shell and AlN core, as theoretically predicted by Hestroffer *et al* [17]. The D^0X_1 peak is sharper, as a clue of a better crystallographic quality or lower impurity concentration, a claim supported by the significant intensity decrease of the 5.95eV contribution for this sample.

However, we observe the emergence of an extremely intense contribution at 5.860 eV. This peak exhibits a fine structure, suggesting that it consists of the convoluted contribution of several radiative sources emitting in the same energy range, namely 5.85 ± 0.5 eV. This contribution is accompanied by two extra peaks at 115 meV and 234 meV lower energy, respectively. These peaks are assigned to phonon replica, consistently with an optical phonon value of 109-117 meV reported in AlN [16].

To our knowledge, the observation of this peak at 5.85 eV has not been previously reported in literature. Although its identification is still unclear, it is worth noting that further investigation using high-resolution transmission electron microscopy (HR-TEM) revealed the presence of basal stacking faults (BSF) in this particular sample (not shown). Therefore, the additional peak may be associated with the existence of BSFs. Interestingly, in the scenario of MBE-grown GaN NWs on a comparable template, the emergence of BSFs has also been observed under metal-rich growth conditions [15]. However a comprehensive study correlating cathodoluminescence with nanostructure is necessary to draw firm conclusions regarding the nature of this contribution.

Thus, it appears that morphology is correlated with the optical quality of the samples. The D^0X_1 peak appears sharper and more intense as the Al/N ratio increases. In addition, the contribution at 5.95eV tends to disappear. Nevertheless, this conclusion should be balanced since sample E (Al-rich growth conditions) exhibits intense, unidentified peaks that are possibly related to extended defects in the AlN lattice. However, at this stage, it is equally possible that these defects are linked to the MEE growth method itself and to the high Al/N effective ratio on the growth front.

Figure 5b shows the sub bandgap contributions, each spectrum corresponding to an ensemble of about 40 nanowires. First, a broad and intense CL band centered at 4.75eV is observed for sample A grown at 950 °C. This peak has been previously observed and assigned to the presence of aluminum vacancies [18]. This observation is consistent with the favorable formation of Al vacancies in N-rich growth conditions. The contribution at 3.52eV is associated with GaN rods, due to shorter length of AlN section compared to the other samples, which leads to additional excitation of GaN base by the electron beam. Considering the offset from the GaN band edge at 5K, it is likely that the GaN is either highly doped or constrained by the AlN shell on the rod [19].

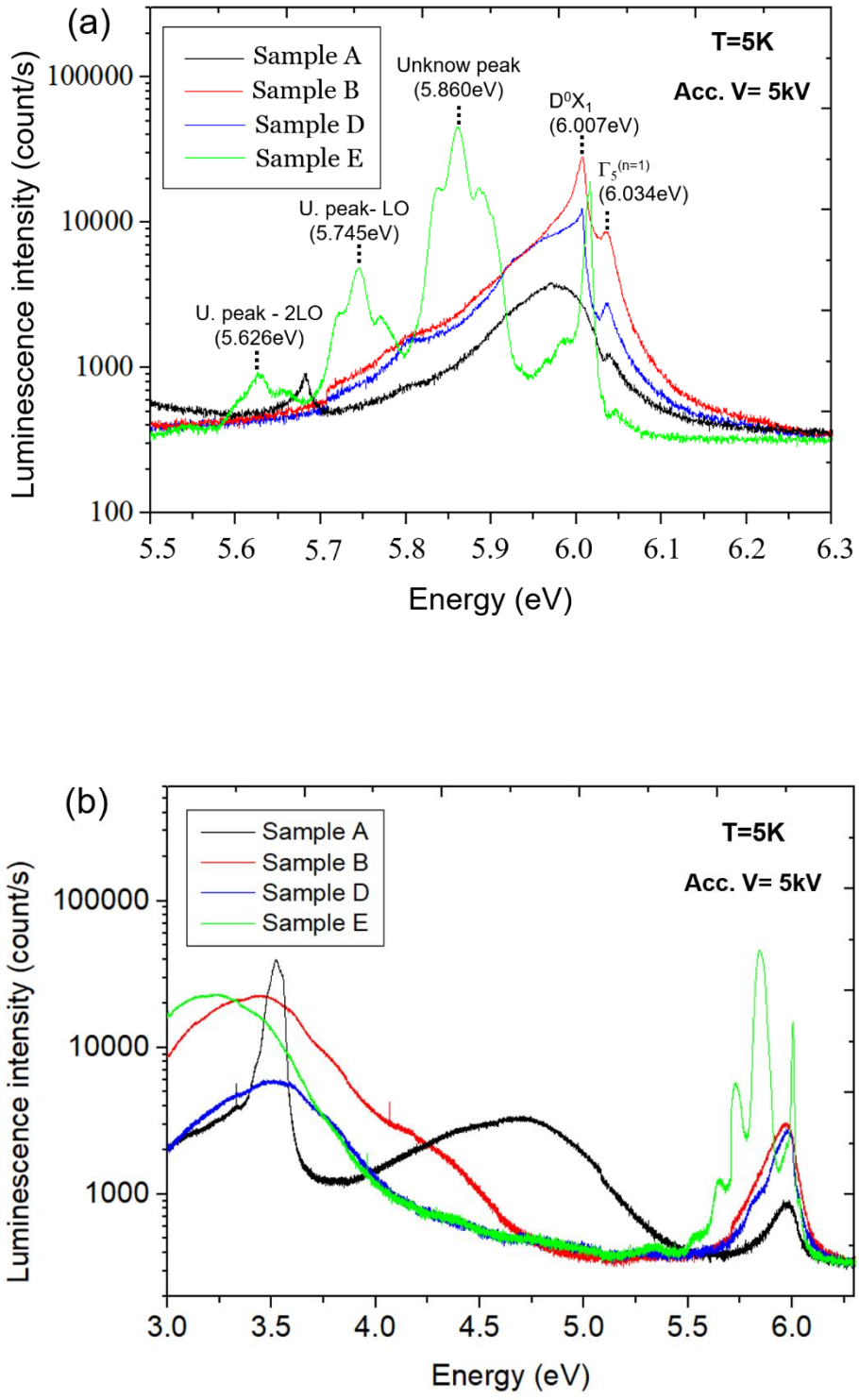

Figure 5: Cathodoluminescence spectra of the studied samples (a) Zoom on the near-band area for a spotted single wire (b) full spectrum acquired on 5x5µm area (about 40 wires). (black) Sample A (blue) Sample D (red) Sample B (green) Sample E.

A broad band is also observed centered around 3.44 eV for both samples B and D. This band is commonly associated with the recombination of a charge carrier on an $O_N - V_{Al}$ complex [18,20], [21].

The shift down to 3.2 eV of this band for sample E could be attributed to the formation of a O-DX center associated with an overall increase in O content in this sample [21]. Indeed, in MEE, the presence of Al excess on the growing surface could favor the gettering of residual O present in the ultra-high vacuum environment of the growth chamber. In addition, it cannot be discarded that the extra peak at 5.85 eV could also be related to an increase in residual O impurities concentration in this sample.

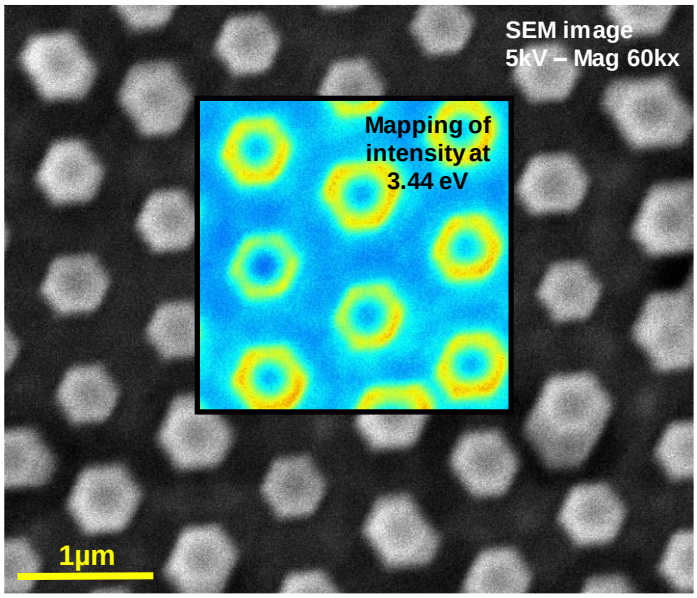

Figure 6 : SEM top-view image of Sample B Inset: CL intensity mapping at 3.44 eV.

In order to check the role of oxygen, energy –filtered CL intensity mapping of sample B was performed, using a photomultiplier tube (PMT). The corresponding CL intensity image recorded at 3.44 eV is shown in the inset in figure 6, superimposed to the top-view SEM image.

Interestingly, it appears that the 3.44 eV emission associated with O presence originates from the periphery of the wires. This suggests that oxygen incorporation into the wires occurs mainly at the periphery, consistent with the pyramidal termination of the NWs put in evidence in figure 1b, which reveals the formation of semi-polar planes. Indeed the preferential incorporation of oxygen on the semi-polar planes has already been observed on MOCVD microwires fir both AlN and GaN [22,23] supporting the attribution of the 3.44 eV emission peak to the similar presence of O in the periphery of MBE-grown AlN NWs.

Conclusion

In conclusion, it appears that the morphology of AlN NWs is governed by diffusion. As diffusion is itself directly linked to Al/N ratio value, we found that this parameter has a major influence on the morphology of AlN nanowires. Increasing the ratio towards Al-rich tends to improve the overall diffusion on all planes. Shifting to a very Al-rich regime using MEE technique resulted in a very flat c-plane and smooth sidewalls deprived of parasitic nucleation on m-planes. We found that a second parameter influencing adatom diffusion, i.e temperature, also has an effect on the morphology of the sidewalls. A growth model that takes into account ESB barriers was proposed to account for the growth of AlN wires by focusing on the extreme cases of AlN nanotube formation on one side and of pyramidal tip-ended NWs on the other side. Furthermore, due to limited Al adatom diffusion and limited Al transfer from sidewalls to top, a very strong influence of the position of the cells relative to the substrate in the chamber was put in evidence. The ratio of longitudinal growth to lateral growth is particularly affected by this factor, opening a path to the possible realization of controlled AlN/GaN or AlN/AlN core/shell structures if properly managing the geometrical arrangement of Al and N cells. We confirmed by cathodoluminescence that the optical quality of our samples improves for increasing Al/V ratio. Finally, the comprehensive identification of the parameters governing optimized AlN NWs morphology and their correlation to optical properties is paving the way to the elaboration of both axial and radial AlN NW-based UV-C emitting opto-electronic devices grown by PA-MBE.

Supporting Information

In supporting information, we describe in detail the calculation of $\frac{\phi_c}{\phi_m}$ and $\frac{III}{V}_m$. The numerical results of these calculations are shown in Table 2.

Acknowlegments The authors acknowledge support from French ANR agency (project ANABASE, ANR-22-CE09-0031). They also acknowledge support from GANEXT (ANR-11-LABX-0014). GANEXT belongs to the public funded “Investissements d’Avenir” program managed by the French ANR agency.

References

(1) Fang, Z.; Robin, E.; Rozas-Jiménez, E.; Cros, A.; Donatini, F.; Mollard, N.; Pernot, J.; Daudin, B. Si Donor Incorporation in GaN Nanowires. *Nano Lett.* **2015**, *15* (10), 6794–6801. https://doi.org/10.1021/acs.nanolett.5b02634.

(2) Glas, F. Critical Dimensions for the Plastic Relaxation of Strained Axial Heterostructures in Free-Standing Nanowires. *Phys. Rev. B* **2006**, *74* (12), 121302. https://doi.org/10.1103/PhysRevB.74.121302.

(3) Landré, O.; Fellmann, V.; Jaffrennou, P.; Bougerol, C.; Renevier, H.; Daudin, B. Growth Mechanism of Catalyst-Free [0001] GaN and AlN Nanowires on Si by Molecular Beam Epitaxy. *Phys. Status Solidi C* **2010**, *7* (7–8), 2246–2248. https://doi.org/10.1002/pssc.200983613.

(4) John, P.; Ruiz, M. G.; van Deurzen, L.; Lähnemann, J.; Trampert, A.; Geelhaar, L.; Brandt, O.; Auzelle, T. Growth Kinetics and Substrate Stability during High-Temperature Molecular Beam Epitaxy of AlN Nanowires. *Nanotechnology* **2023**, *34* (46), 465605. https://doi.org/10.1088/1361-6528/acefd8.

(5) Zhao, S.; Connie, A. T.; Dastjerdi, M. H. T.; Kong, X. H.; Wang, Q.; Djavid, M.; Sadaf, S.; Liu, X. D.; Shih, I.; Guo, H.; Mi, Z. Aluminum Nitride Nanowire Light Emitting Diodes: Breaking the Fundamental Bottleneck of Deep Ultraviolet Light Sources. *Sci. Rep.* **2015**, *5* (1), 8332. https://doi.org/10.1038/srep08332.

(6) Mi, Z.; Zhao, S.; Woo, S. Y.; Bugnet, M.; Djavid, M.; Liu, X.; Kang, J.; Kong, X.; Ji, W.; Guo, H.; Liu, Z.; Botton, G. A. Molecular Beam Epitaxial Growth and Characterization of Al(Ga)N Nanowire Deep Ultraviolet Light Emitting Diodes and Lasers. *J. Phys. Appl. Phys.* **2016**, *49* (36), 364006. https://doi.org/10.1088/0022-3727/49/36/364006.

(7) Bavencove, A.-L.; Tourbot, G.; Garcia, J.; Désières, Y.; Gilet, P.; Levy, F.; André, B.; Gayral, B.; Daudin, B.; Dang, L. S. Submicrometre Resolved Optical Characterization of Green Nanowire-Based Light Emitting Diodes. *Nanotechnology* **2011**, *22* (34), 345705. https://doi.org/10.1088/0957-4484/22/34/345705.

(8) Hestroffer, K.; Daudin, B. A Geometrical Model for the Description of the AlN Shell Morphology in GaN-AlN Core-Shell Nanowires. *J. Appl. Phys.* **2013**, *114* (24), 244305. https://doi.org/10.1063/1.4854495.

(9) van Treeck, D.; Fernández-Garrido, S.; Geelhaar, L. Influence of the Source Arrangement on Shell Growth around GaN Nanowires in Molecular Beam Epitaxy.

Phys. Rev. Mater. **2020**, *4* (1), 013404. https://doi.org/10.1103/PhysRevMaterials.4.013404.

(10) Liu, S. J.; Huang, H.; Woo, C. H. Schwoebel-Ehrlich Barrier: From Two to Three Dimensions. *Appl. Phys. Lett.* **2002**, *80* (18), 3295–3297. https://doi.org/10.1063/1.1475774.

(11) Neugebauer, J.; Zywietz, T. K.; Scheffler, M.; Northrup, J. E.; Chen, H.; Feenstra, R. M. Adatom Kinetics On and Below the Surface: The Existence of a New Diffusion Channel. *Phys. Rev. Lett.* **2003**, *90* (5), 056101. https://doi.org/10.1103/PhysRevLett.90.056101.

(12) Zywietz, T.; Neugebauer, J.; Scheffler, M. Adatom Diffusion at GaN (0001) and (000$\bar{1}$) Surfaces. *Appl. Phys. Lett.* **1998**, *73* (4), 487–489. https://doi.org/10.1063/1.121909.

(13) Lee, C. D.; Dong, Y.; Feenstra, R. M.; Northrup, J. E.; Neugebauer, J. Reconstructions of the AlN(0001) Surface. *Phys. Rev. B* **2003**, *68* (20), 205317. https://doi.org/10.1103/PhysRevB.68.205317.

(14) Lymperakis, L.; Neugebauer, J. Large Anisotropic Adatom Kinetics on Nonpolar GaN Surfaces: Consequences for Surface Morphologies and Nanowire Growth. *Phys. Rev. B* **2009**, *79* (24), 241308. https://doi.org/10.1103/PhysRevB.79.241308.

(15) Gruart, M.; Jacopin, G.; Daudin, B. Role of Ga Surface Diffusion in the Elongation Mechanism and Optical Properties of Catalyst-Free GaN Nanowires Grown by Molecular Beam Epitaxy. *Nano Lett.* **2019**, *19* (7), 4250–4256. https://doi.org/10.1021/acs.nanolett.9b00023.

(16) van Deurzen, L.; Singhal, J.; Encomendero, J.; Pieczulewski, N.; Chang, C.; Cho, Y.; Muller, D. A.; Xing, H. G.; Jena, D.; Brandt, O.; Lähnemann, J. Excitonic and Deep-Level Emission from N- and Al-Polar Homoepitaxial AlN Grown by Molecular Beam Epitaxy. arXiv May 17, 2023. https://doi.org/10.48550/arXiv.2305.10542.

(17) Hestroffer, K.; Mata, R.; Camacho, D.; Leclere, C.; Tourbot, G.; Niquet, Y. M.; Cros, A.; Bougerol, C.; Renevier, H.; Daudin, B. The Structural Properties of GaN/AlN Core–Shell Nanocolumn Heterostructures. *Nanotechnology* **2010**, *21* (41), 415702. https://doi.org/10.1088/0957-4484/21/41/415702.

(18) Bastek, B.; Bertram, F.; Christen, J.; Hempel, T.; Dadgar, A.; Krost, A. Analysis of Point Defects in AlN Epilayers by Cathodoluminescence Spectroscopy. *Appl. Phys. Lett.* **2009**, *95* (3), 032106. https://doi.org/10.1063/1.3154518.

(19) Rigutti, L.; Jacopin, G.; Largeau, L.; Galopin, E.; De Luna Bugallo, A.; Julien, F. H.; Harmand, J.-C.; Glas, F.; Tchernycheva, M. Correlation of Optical and Structural Properties of GaN/AlN Core-Shell Nanowires. *Phys. Rev. B* **2011**, *83* (15), 155320. https://doi.org/10.1103/PhysRevB.83.155320.

(20) Weinstein, I. A.; Vokhmintsev, A. S.; Spiridonov, D. M. Thermoluminescence Kinetics of Oxygen-Related Centers in AlN Single Crystals. *Diam. Relat. Mater.* **2012**, *25*, 59–62. https://doi.org/10.1016/j.diamond.2012.02.004.

(21) Koppe, T.; Hofsäss, H.; Vetter, U. Overview of Band-Edge and Defect Related Luminescence in Aluminum Nitride. *J. Lumin.* **2016**, *178*, 267–281. https://doi.org/10.1016/j.jlumin.2016.05.055.

(22) Valera, L.; Jaloustre, L.; Reita, V.; De Mello, S. R. S.; Bellet-Amalric, E.; Petit-Étienne, C.; Pargon, E.; Jacopin, G.; Durand, C. Organized AlN Nanowire Arrays by Hybrid Approach of Top-Down Processing and MOVPE Overgrowth for Deep UV Emission Devices. *ACS Appl. Nano Mater.* **2024**, *7* (9), 10338–10349. https://doi.org/10.1021/acsanm.4c00814.

(23) Cruz, S. C.; Keller, S.; Mates, T. E.; Mishra, U. K.; DenBaars, S. P. Crystallographic Orientation Dependence of Dopant and Impurity Incorporation in GaN Films Grown by Metalorganic Chemical Vapor Deposition. *J. Cryst. Growth* **2009**, *311* (15), 3817–3823. https://doi.org/10.1016/j.jcrysgro.2009.02.051.